The Design of Rotation-Invariant Pattern Recognition Using the Silicon Retina

Chin-Fong Chiu, *Member, IEEE,* and Chung-Yu Wu, *Senior Member, IEEE*

***Abstract*—A new rotation-invariant pattern recognition system is proposed and analyzed. In this system, silicon retina cells capable of image sensing and edge extraction are used so that the system can directly process images from the real world without an extra edge detector. The rotation-invariant discrete correlation function is modified and implemented in the silicon retina structure by using the current summation. Simulation results have verified the correct function of the proposed system. Moreover, an experimental chip to implement the proposed system with a 32 × 32 cell array has been designed and fabricated in 0.8-μm n-well CMOS process. Experimental results have successfully shown that the system works well for the arbitrary orientation pattern recognition.**

***Index Terms*— Circular harmonic transformation, rotation-invariant, silicon retina.**

I. Introduction

In recent years, the study of artificial neural networks has become one of the main research efforts [1]–[2]. The general purpose of artificial neural networks is to realize the major functions of human auditory, visual, and neural systems. In the realization of human visual functions, the development of pattern recognition techniques is the first step to make the networks capable of understanding and reacting to the visual inputs.

The conventional pattern recognition methods require input patterns to be presented in standard position, orientation, size, etc. But the input patterns from the real world may be shifted, rotated, or scale-changed. Moreover, they may contain noise or uncorrelated data. To restore the shifted or the scale-changed patterns, some automatic image control systems have been proposed to move the image sensor to the correct position or adjust the size of input object patterns [3]–[6]. However, the orientations of arbitrarily rotated patterns still cannot be restored by the conventional image control systems before recognizing them.

So far, many neural network systems designed to perform recognition invariant to the pattern orientations have been proposed [7]–[11]. Some of them, however, fail to recognize the arbitrary orientations of input patterns [7]–[9]. Others [10], [11] may result in very time-consuming operations and may not be suitable for real-time processing.

Another approach which has been proposed for orientation-invariant pattern recognition is to use the similarity criterion defined by certain mathematical transformations [12]–[19] which can be calculated and implemented by computer software. One of the transformations is the circular harmonic transformation [15]–[19]. In this transformation, the correlation function in the polar coordinates, which correlates an arbitrarily rotated image with the circular harmonic component of the reference image, is invariant to rotation. If the rotation-invariant correlation function is further expressed in the discrete domain, it becomes the weighted summation of the image data [19]. The weighting factors are circular harmonic components obtained from the circular harmonic transformation of the reference image. For real-time image processing applications, the discrete correlation function should be realized in very large scale integration (VLSI) hardware.

In this paper, the rotation-invariant discrete correlation function is modified for VLSI implementation and a rotation-invariant pattern recognition system is designed in CMOS technology and measured. In the modified correlation function, only the zeroth harmonic component is used to remove the phase term. Thus, the discrete correlation function of an arbitrarily rotated image becomes the multiplication of a weight and the sum of the image data on the concentric circle. In the realization of the rotation-invariant pattern recognition system, the CMOS silicon retina [20], [21] is used for image detection and edge extraction. The modified discrete correlation function can be compactly implemented on the output emitter currents of the silicon retina. The experimental chip has been measured and characterized. The results have verified the correct rotation invariance of the proposed system.

In Section II, the rotation-invariant principle of the circular harmonic transformation is reviewed and the discrete rotation-invariant correlation function is derived with modification for VLSI implementation. The circuit architecture and operational principle of the proposed system are described in Section III. In Section IV, the simulation results of the system are presented, and the recognition errors are analyzed. The experimental results are presented and discussed in Section V. In Section VI, the conclusion is given.

II. Modified Rotation-Invariant Circular Harmonic Transformation

In this section, the modified rotation-invariant circular harmonic transformation will be developed for VLSI implemen-

Manuscript received February 19, 1996; revised November 5, 1996. This work was supported by the National Science Council, Taiwan, R.O.C., under Contract NSC82-0416-E-009-212.

C.-F. Chiu is with the Chip Implementation Center (CIC), National Science Council, Hsinchu, Taiwan 300, R.O.C.

C.-Y. Wu is with the Integrated Circuits and Systems Laboratory, Department of Electronics Engineering, Institute of Electronics, National Chiao-Tung University, Hsinchu, Taiwan 300, R.O.C.

Publisher Item Identifier S 0018-9200(97)02467-0.

tation. According to the circular harmonic expansion [16] in polar coordinates with radius r and angle θ in radians, an image pattern $f(r,\theta)$ may be decomposed into circular harmonic components as

$$f(r,\theta)=\sum_{M=-\infty}^{\infty} f_M(r)e^{jM\theta} \tag{1}$$

where

$$f_M(r)=\frac{1}{2\pi}\int_0^{2\pi} f(r,\theta)e^{-jM\theta}d\theta. \tag{2}$$

If this image pattern is rotated by α radians, the rotated components can be expressed as

$$f(r,\theta+\alpha)=\sum_{M=-\infty}^{\infty} f_M(r)e^{jM\theta}e^{jM\alpha}. \tag{3}$$

When the rotated image pattern is correlated with one of the circular harmonic components in $f(r,\theta)$, the correlation value $C(r_i,\alpha)$ at $r=r_i$ can be expressed as

$$\begin{aligned} C(r_i,\alpha) &= f(r_i,\theta+\alpha)\otimes f_M(r_i)e^{jM\theta} \\ &\equiv \int_0^{2\pi} f(r_i,\theta+\alpha)f_M^*(r_i)e^{-jM\theta}d\theta \end{aligned} \tag{4}$$

where "$\otimes$" is the correlation operation, and $f_M^*(r_i)$ is the complex conjugate of $f_M(r_i)$. Substituting (3) into (4) yields

$$|C(r_i,\alpha)|=\left|2\pi e^{jM\alpha}|f_M(r_i)|^2\right|=2\pi|f_M(r_i)|^2. \tag{5}$$

It can be realized from (5) that the magnitude of $C(r_i,\alpha)$ is independent of the image orientation α. Thus, it can be used as an indicator to identify and recognize the rotated image patterns.

In the above transformation, the rotated image is correlated with the circular harmonic component of the original image. In fact, the rotation invariance still exists when the circular harmonic component of an image pattern is correlated with an arbitrary image $g(r,\theta)$ [19]. The correlation function $R(r,\theta)$ at $r=r_i$ of $g(r_i,\theta)$ with the circular harmonic component of $f(r_i,\theta)$ can be expressed as

$$R(r_i,\theta)=g(r_i,\theta)\otimes[f_M(r_i)e^{jM\theta}]. \tag{6}$$

Rotating the image $g(r,\theta)$ by α radians, the correlation function can be expressed as

$$\begin{aligned} R_1(r_i,\theta) &= g(r_i,\theta+\alpha)\otimes\left[f_M(r_i)e^{jM\theta}\right] \\ &= e^{jM\alpha}R(r_i,\theta+\alpha). \end{aligned} \tag{7}$$

This proves that even when an arbitrary object image is rotated, the magnitude of its correlation function with the circular harmonic component of the reference image $f(r,\theta)$ remains the same.

To implement the correlation function in VLSI, a discrete transformation is introduced to approximate the circular harmonic components of $f(r,\theta)$ in (2) [19]. The resultant expression is

$$f_M(r_i)=\frac{1}{L_i}\sum_{n=0}^{L_i-1} f(r_i,\theta_n)e^{-jM\theta_n},\quad i=1,\cdots,N \tag{8}$$

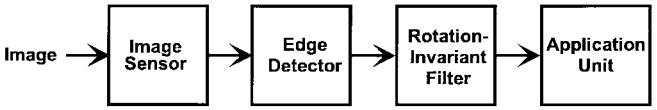

Fig. 1. The block diagram of the typical rotation-invariant pattern recognition system.

where r_i is the discrete radius, L_i is the number of pixels with the radius r_i, and θ_n is the discrete angle given by $\theta_n=2\pi n/L_i$. For the ease of VLSI implementation, only the zeroth circular harmonic component is selected. Then the correlation function at the specific concentric circle r_i can be obtained from (7) with $r=r_i$ and $M=0$ as

$$R(r_i,\theta)=g(r_i,\theta)\otimes f_0(r_i) \tag{9}$$

Substituting the expression of $f_0(r_i)$ in (8) into (9), we have

$$\begin{aligned} R(r_i)=R(r_i,\theta) &= \sum_{n=0}^{L_i-1} g(r_i,\theta_n)f_0(r_i) \\ &= f_0(r_i)\sum_{n=0}^{L_i-1} g(r_i,\theta_n) \end{aligned} \tag{10}$$

where

$$f_0(r_i)=\frac{1}{L_i}\sum_{n=0}^{L_i-1} f(r_i,\theta_n). \tag{11}$$

In (10), it is shown that the rotation-invariant correlation function $R(r_i,\theta)$ of an arbitrary image $g(r,\theta)$ is independent of the angle θ_n. Thus it can be rewritten as $R(r_i)$. $R(r_i)$ can be expressed as the multiplication of $f_0(r_i)$ with the sum of the image data on the concentric circle $r=r_i$. In practice, the recognition performance of the proposed system can be tuned through the adjustment on the value of $f_0(r_i)$.

III. Circuit Architecture and Operational Principle

Fig. 1 shows the typical structure of a rotation-invariant recognition system. It consists of an image sensor to sense the input image and edge detector to extract the edge of the input image pattern and suppress noise or undesired data. Then the edge patterns are sent to a preprocessor called the rotation-invariant filter which performs the modified discrete correlation function to identify the rotated patterns. Finally, all the rotated patterns are classified and the results may be sent to the application unit for further processing or applications.

The image sensor, edge detector, and rotation-invariant filter in Fig. 1 can be realized compactly by using the silicon retina [20]–[21]. Fig. 2(a) shows the row decoder, digital image data input, and part of the silicon retina cell array, whereas Fig. 2(b) shows the cell array, multiplexer, and output amplifier. The silicon retina cell circuitry is shown in Fig. 2(c). In Fig. 2(c), the silicon retina which consists of one inner p-n-p bipolar junction transistor (BJT) and one outer p-n-p BJT, is used to sense the image and detect the edge at the same time [20]–[21]. To increase the flexibility and testability of the rotation-invariant recognition system, a latch is designed in each cell to latch the digital edge image data, as shown in Fig. 2(c). The switches SW3 and SW4 control the input type.

When SW3 is closed and SW4 is open, the digital edge image data stored in the latch is used. Conversely, when SW4 is closed and SW3 is open, the image sensed by the silicon retina is used. Note that when the digital image is used, no light is incident on the silicon retina. The small dark current of the outer p-n-p can be neglected. Thus, no switch is used to disconnect the outer p-n-p BJT from the output.

In Fig. 2(c), the latch circuit contains two inverters and two switches. The latch input is controlled by the row decoder. In Fig. 2(a), the row decoder decodes the m row address bits and activates one of the 2^m row control signals *row* and $\overline{row}$. The digital edge image data can be input to the latch row-by-row by sending a sequence of row address bits. The row control signals *row* and $\overline{row}$ control two switches in the latch circuit. When one row is selected by the row address bits, the control signal *row* of the selected row is activated to high, whereas $\overline{row}$ is low. Thus, SW1 is closed to change the latched signal to the input signal and SW2 is open to prevent the feedback of the latched signal. In the deselected row, *row* is low and $\overline{row}$ is high. Thus, SW1 is open and SW2 is closed to store the input image signal.As shown in Fig. 2(c), the latched signal controls the current source. When the latched signal is high, the current source is connected to the switch SW3. Through SW3 and the multiplexer in Fig. 2(b), the current source may be further connected to the inputs of the R_m amplifier. The input of the R_m amplifiers is kept at virtual ground. Thus, the current of the current source can be kept constant. Since the switch SW4 is open, the current of the current source does not affect the inner p-n-p BJT.

To obtain the image data from the real world, the silicon retina cell is used. As shown in Fig. 2(c), the basic cell of the silicon retina contains an inner open-base parasitic p-n-p phototransistor as the photoreceptor and an outer open-base parasitic p-n-p phototransistor in the common N-well as the smoothing unit [20]–[21]. When the light is incident upon the common N-well base region, the generation of excess carriers results in the base current. The base current flowing through the emitter junction leads to decreasing emitter junction voltages with distance. Thus, the output emitter currents decay logarithmically with distance which realizes the smoothing function. The smoothed signal of the input image can be obtained from the emitter current of the outer phototransistor, whereas the signal of the original image can be obtained from the emitter current of the inner phototransistor. The subtraction of these two emitter currents results in a difference signal with a sharp change at the edge of the image. Thus, the edge signal of the image can be detected definitely.

The silicon retina not only can transform the light signal into the current, but can simultaneously extract the edge of the pattern. Thus, the output signal of the silicon retina can be directly used without designing an extra preprocessor to extract the edge of the pattern. This can save a large chip area and increase the cell density and the fill factor if on-chip edge detection is to be performed in the focal plane. The emitter of the inner phototransistor of the silicon retina is connected to SW4. Through SW4 and the multiplexer in Fig. 2(b), the emitter current of the inner phototransistors are further connected to the input of the R_m amplifiers. The emitter of the outer phototransistor is connected to the other R_m amplifier through the multiplexer. Since the inputs of the R_m amplifiers are kept at virtual ground, the phototransistors can be biased in the active region.

From (10), the rotation-invariant correlation function can be expressed as the multiplication of a constant weight with the sum of the image data on the same concentric circle. In the experimental chip, the cell at (15, 15) in the 32 $\times$ 32 cell array is defined as the center and the 32 $\times$ 32 cell array in Cartesian coordinates is transformed into a circular array with radius 15 in polar coordinates. The cells outside the circular array are not used because their associated concentric circles are not complete. The circular array is further divided into five groups of concentric circles and each group consists of three successive concentric circles which are assumed to have the same weighting factor. Thus, the rotation-invariant correlation functions of the three concentric circles in each group can be summed together to form the correlation function output of the group. The five groups generate five rotation-invariant correlation function outputs, each of which can be expressed for the input image $g(r,\theta)$ as

$$V_{\text{out}}(r_i) = f_0(r_i)\left[\sum_{n=0}^{L_i-1} g(r_i,\theta_n) + \sum_{n=0}^{L_i-1} g(r_{i+1},\theta_n) + \sum_{n=0}^{L_i-1} g(r_{i+2},\theta_n)\right]. \tag{12}$$

Comparing to (10), $V_{\text{out}}(r_i)$ is equivalent to the correlation function $R(r_i)$. Hence, $V_{\text{out}}(r_i)$ is rotation-invariant.

To realize the function $V_{\text{out}}(r_i)$ in (12), the outputs of all current sources or the emitters of inner p-n-p BJT's on the same concentric circle are connected together in the cell array shown in Fig. 2(b). Thus, through SW3 or SW4, their output currents which represent $g(r_i,\theta_n)$ can be summed together. Then the outputs of three concentric circles in the same group are connected together to realize (12). Similarly, the emitters of outer p-n-p BJT's on the same concentric circle are connected together, and then the outputs of three concentric circles are connected together to form the other output of the group. Thus, each group has two outputs which are sent to the multiplexer. Each time, only one set of outputs out of the five sets of outputs from the five groups of concentric circles can be selected and sent to the R_m amplifier as shown in Fig. 2(b).

Since the edge of the pattern image is extracted by the subtraction of two emitter currents in the silicon retina, the subtraction of the currents at the two outputs selected by the multiplexer should be performed. This is realized by the differential output buffer which subtracts the output voltages of the two R_m amplifiers as shown in Fig. 2(b). Since the currents are transformed into V_{out} via R_m amplifier with the transconductance R_m and output buffer with the voltage gain A_v, $f_0(r_i)$ in (12) can be expressed as

$$f_0(r_i) = -A_v R_m. \tag{13}$$

The circuit diagrams of the R_m amplifier and the output buffer are shown in Fig. 3(a) and (b), respectively. As shown

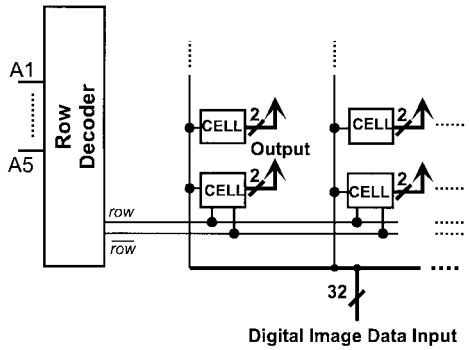

(a)

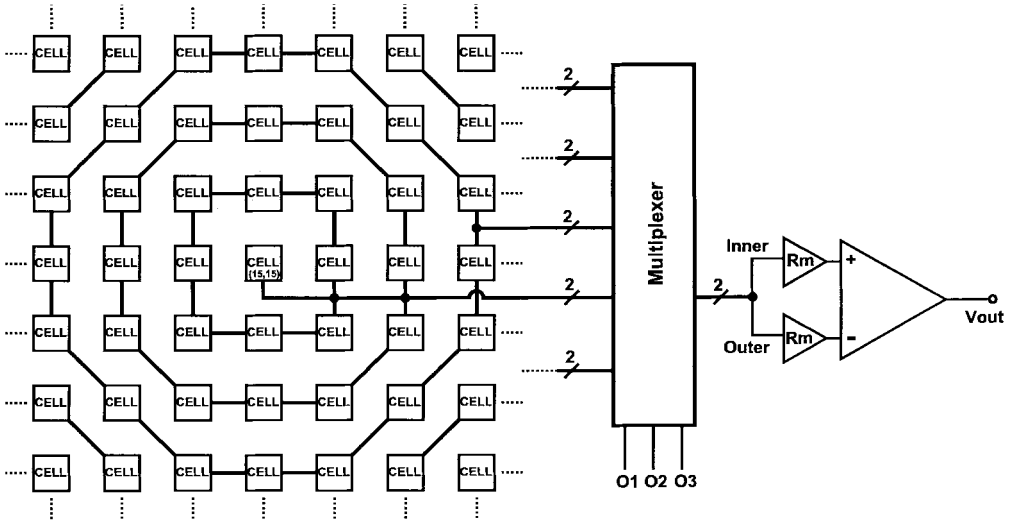

(b)

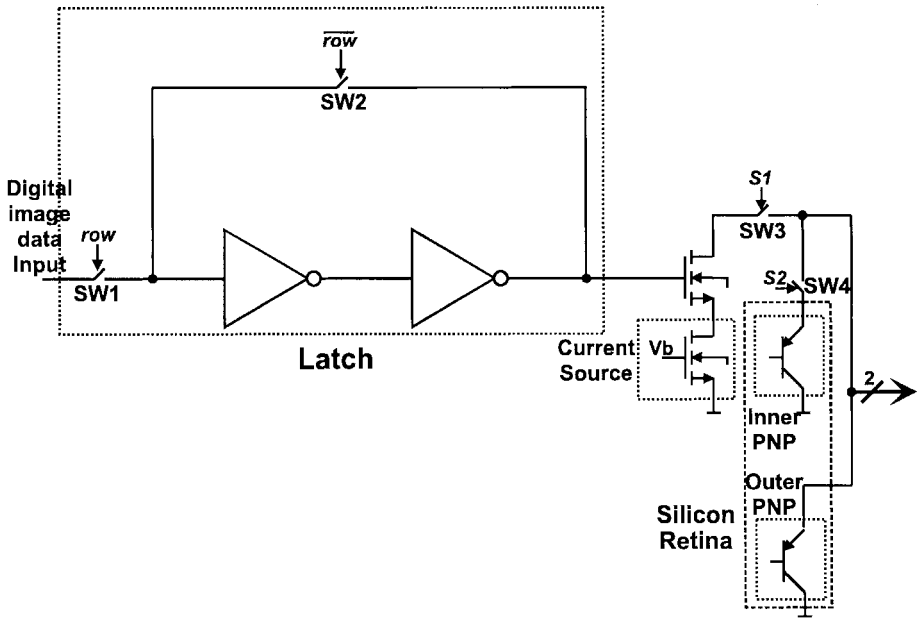

(c)

Fig. 2. (a) Row decoder, digital image data input, and cell array, (b) whole cell array, multiplexer, and output amplifier, and (c) cell circuitry of the proposed rotation-invariant pattern recognition system.

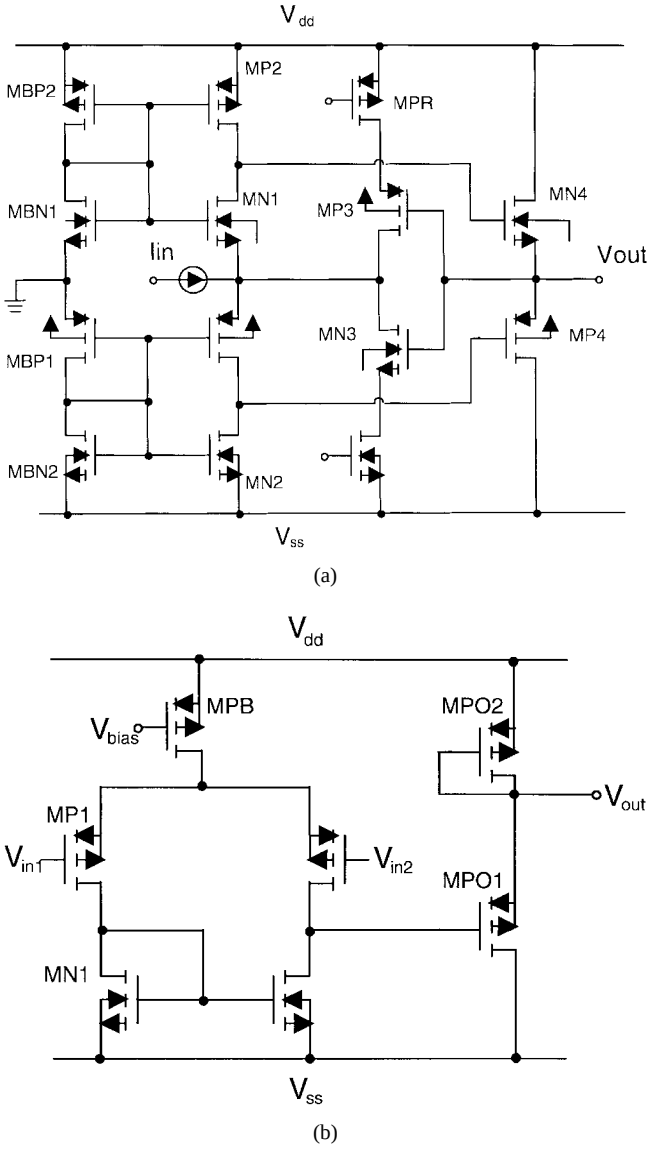

Fig. 3. The circuit diagrams of (a) the CMOS wideband R_m amplifier and (b) the CMOS output buffer used in the proposed system.

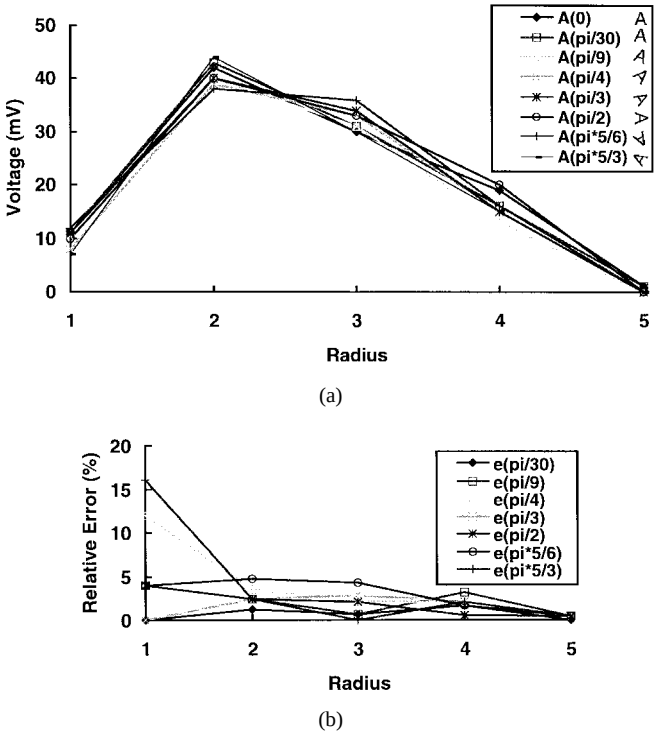

Fig. 4. (a) The simulated output voltages versus radius for different patterns of "A" rotated by different angles as denoted by $A(\theta)$. (b) The relative errors for different rotated patterns of "A" as derived from (a).

in Fig. 3(a), the basic I-V conversion of the R_m amplifier is achieved by the common-gate transistor MN1(MP1) and the current source device MP2(MN2). The transistors MN4 and MP4 form a source-follower output buffer to enhance the driving capability and decrease the output impedance. The transistors MN3 and MP3 offer a shunt-shunt feedback path from the output stage to reduce both input and output impedance. The transistors MNR and MPR are used to adjust the gain of the R_m amplifier so that the weight $f_0(r_i)$ in (13) can be tuned to optimize the system performance. It is shown that the R_m amplifier has a very low input impedance, a good linearity, and a large bandwidth [22].

The output buffer in Fig. 3(b) consists of a basic differential amplifier and a source-follower. The differential amplifier produces an output voltage that is proportional to the output voltage difference of the two R_m amplifiers. The source-follower offers a large driving capability to drive the output pads.

IV. Simulation Results and Error Analysis

To verify the rotation invariance of the proposed system, simulations on some digital patterns have been performed. Fig. 4(a) shows the simulated output voltages versus the radii of five groups of concentric circles for eight different input patterns of English letter "A" which are rotated by $0,\ \pi/30, \pi/9,\ \pi/4,\ \pi/3,\ \pi/2,\ 5\pi/6$ and $5\pi/3$. From Fig. 4(a), it can be seen that the maximum deviation among the output voltages of different patterns is smaller than 10 mV. Thus, they can be identified as the unique feature of the arbitrarily rotated letter "A." To further analyze the deviations, the relative errors with respect to the nonrotated letter "A" are shown in Fig. 4(b). The relative error is defined as the error divided by the number of pixels in the concentric circle group. It can be seen that the relative error is below 15%, and the average error over five radii is below 5%. The simulated output voltages of the unrotated letters "B," "C," and "A" are shown in Fig. 5. As compared Figs. 5 with 4, it can be realized that the difference between letter "A" and "B"/"C" is more significant than that among the rotated "A." Thus, the rotation invariance of the proposed system can be verified.

There are two possible error sources in the proposed system. One is the spatial sampling error which consists of the spatial mismatching error due to the transformation from the Cartesian coordinates to the polar coordinates and the spatial error due to spatial discretization. In the design of Fig. 2(b), the spatial mismatching error is more significant than the spatial error. Generally, the spatial error due to spatial discretization may be reduced by using a larger sensor array. The spatial mismatching error is a result of an imperfect match between

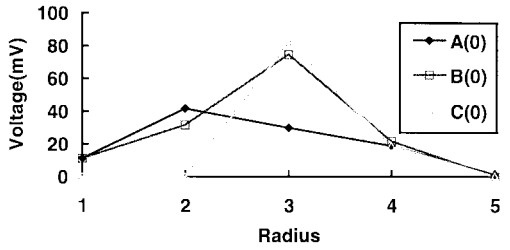

Fig. 5. The simulated output voltages versus radius for different letters "A," "B," and "C."

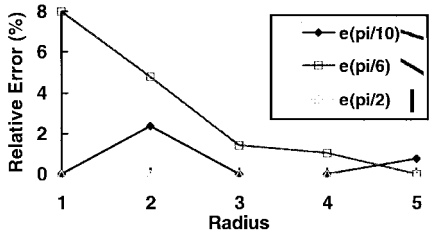

Fig. 6. The simulated relative errors versus radius for different light-bar patterns rotated by different angles.

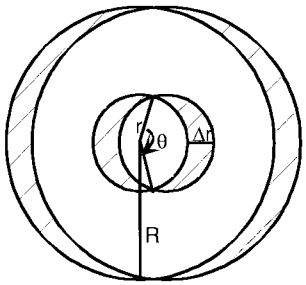

Fig. 7. The conceptual diagram of two rings of concentric circles with their centers shifted by Δr. The resultant maximum mismatch errors are shown by the shaded parts.

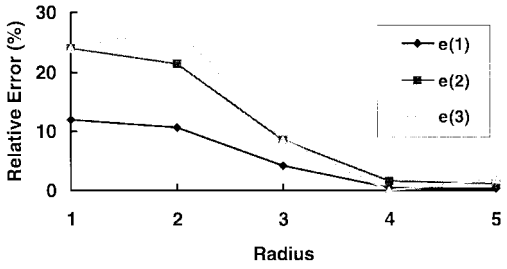

Fig. 8. The simulated relative errors for the patterns of the letter "A" shifted from the center one, two, and three pixels. The corresponding relative errors are denoted by $e(n)$ with $n = 1, 2, 3$.

the rectangular grids used in the spatial sampling of the image and the polar grids used in forming the discrete correlation function. To further analyze the spatial mismatching error, a set of light bars rotated by 0, $\pi/10$, $\pi/6$, and $\pi/2$ are used in the simulation of this system. As shown in Fig. 6, the simulated relative errors are mainly due to the spatial sampling errors. In Fig. 6, it is found that no error occurs when the light bar is rotated by $\pi/2$. This is due to the symmetric property between X axis and Y axis in the Cartesian coordinates. In general, the spatial sampling errors become significant in the area close to the center of the polar coordinates as shown in Figs. 4 and 6. This is because the nearer the circle is to the center, the less the points are on the concentric circle. Therefore, the positions of image sensors in the rotation-invariant pattern recognition system should be arranged in polar coordinates to minimize the spatial sampling error. Moreover, the array size, the array resolution, and the image size should be large enough to minimize the spatial error due to spatial discretization.

The other error is caused by the shift of the center of the input pattern from the array center pixel (15, 15), namely the center of the polar coordinates. The center mismatch error is illustrated in Fig. 7 where the centers of two concentric rings are shifted by Δr. The maximum error between correct and shifted outputs is represented by the shaded part in Fig. 7. The relative error of the mismatch centers can be expressed as the ratio between the ring area and the shaded area as shown by (14), at the bottom of the page. For the fixed system resolution, the larger the $(R - r)$ is, the smaller the error value is. However, increasing the width of the ring reduces the number of correlation function outputs since the total pixel number is constant. Fig. 8 shows the simulated mismatch errors when the input pattern "A" is shifted by one, two, and three pixels with respect to the center of the system. The error of the shifted patterns becomes more evident when the shifted distance is longer. However, the error can be minimized by adjusting the transresistance of the R_m amplifier, that is, the weight function $f_0(r_i)$.

In fact, increasing the system resolution is more efficient in minimizing the relative error. To analyze the relation between error and resolution, a system which consists of 128 $\times$ 128 cells is simulated. In the simulated system, the circular array with 60 radii is divided into five concentric circle groups, and each group includes 12 successive concentric circles. As comparing the simulated relative spatial errors with those in Fig. 4(b), the maximum relative error decreases from 16% to below 2.5%. As comparing the mismatch errors with those in Fig. 8, the maximum relative error decreases from 24% to below 6%. Thus, the relative errors can be significantly reduced in the high resolution system.

$$e = \frac{\text{Area}_{\text{shaded}}}{\text{Area}_{\text{ring}}} = \frac{(2R^2 - 2r^2)(\pi - \theta) + 2\Delta r\sqrt{r^2 - \left(\frac{\Delta r}{2}\right)^2} + 2\Delta r\sqrt{R^2 - \left(\frac{\Delta r}{2}\right)^2}}{\pi(R^2 - r^2)}$$
$$= \frac{2(\pi - \theta)(R + r)}{\pi(R - r)} - \frac{4Rr(\pi - \theta)}{\pi(R - r)(R + r)} + \frac{2\Delta r\left(\sqrt{r^2 - \left(\frac{\Delta r^2}{2}\right)} + \sqrt{R^2 - \left(\frac{\Delta r^2}{2}\right)}\right)}{\pi(R - r)(R + r)} \tag{14}$$

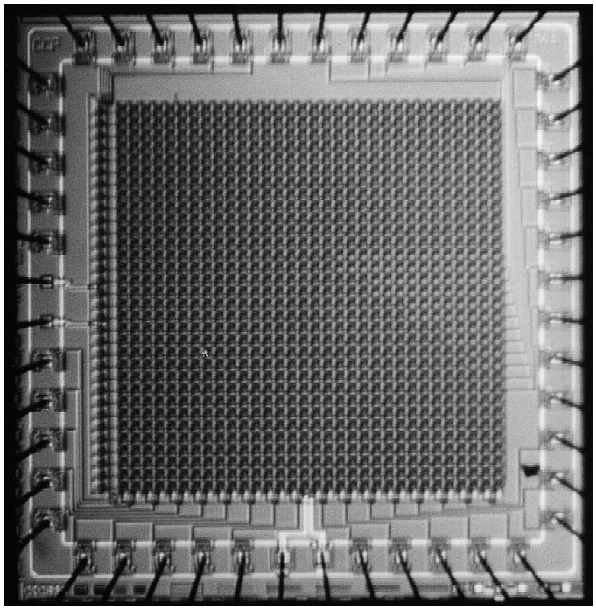

Fig. 9. The chip photograph of the proposed system.

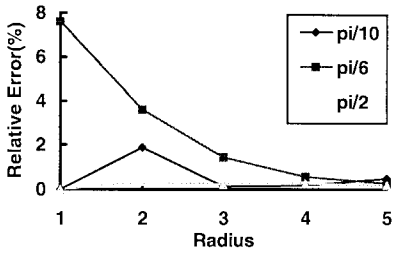

Fig. 10. The measured relative errors for different digital light-bar patterns rotated by $0,\ \pi/10,\ \pi/6$, and $\pi/2$.

V. Measurement Results

The experimental chip is fabricated in 0.8-μm n-well CMOS process. Fig. 9 shows the chip photograph. In this initial testing chip, the cells are arranged in Cartesian coordinates for layout convenience and testing purpose. The area of the cell including silicon retina, latch, and switches is $110 \times 110\ \mu\text{m}^2$. In practical application, the cell may contain only the silicon retina whose area is $40 \times 40\ \mu\text{m}^2$, and the cell array should be arranged in polar coordinates. As to the digital latch and switches, they are used for testing purpose.

To measure the rotation invariance, the digital patterns of light bars with five-pixel width and rotated by $\pi/10,\ \pi/6,\ \pi/2$ are input to the fabricated chip, and the output voltages are measured. Fig. 10 shows the measured relative errors of the rotated patterns. From Fig. 10, it can be seen that the measured errors between the unrotated light bar and the light bar rotated by $\pi/2$ are less than 1%, whereas those between the unrotated and $\pi/6$ rotated patterns are relatively larger. As may be realized from Fig. 6 and the analysis in Section IV, the measured errors are mainly due to the spatial sampling errors.

To further verify the function of the fabricated rotation-invariant system, more complicated digital image patterns are tested. Fig. 11 shows the measured output voltages of the

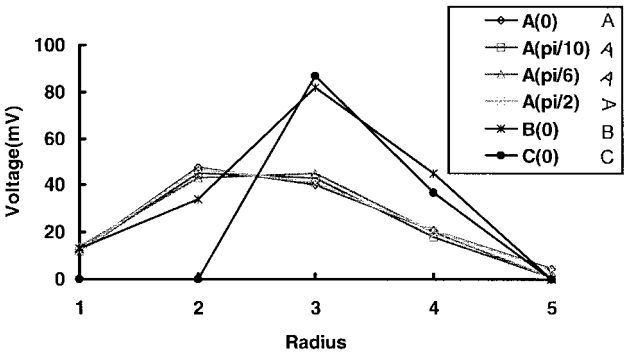

Fig. 11. The measured output voltages versus radius for digital patterns of "A," "B," and "C" as rotated digital patterns of "A."

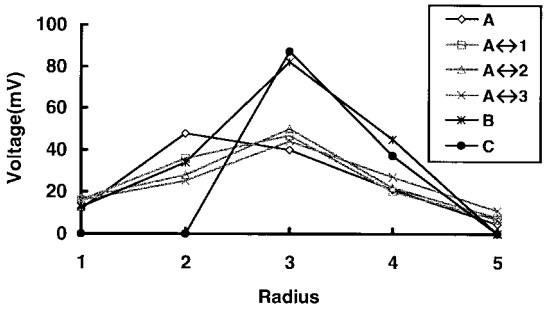

Fig. 12. The measured output voltages versus radius for digital patterns of "A," "B," and "C" as well as digital patterns of "A" shifted by one, two, and three pixels from the center of cell array.

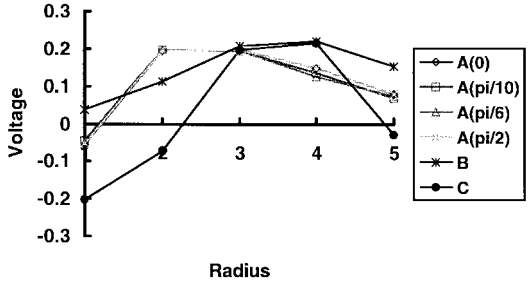

Fig. 13. The measured output voltages versus radius for the real image patterns of "A," "B," "C," and the rotated "A," all sensed directly by the silicon retina.

digital patterns of the English letters "A," "B," and "C" as well as the patterns of "A" rotated by $\pi/10,\ \pi/6$, and $\pi/2$. It is seen that the four curves of the rotated "A" patterns are very similar, whereas those of the letters "A," "B," and "C" have a significant difference. This verifies the correct function of the proposed rotation-invariant pattern recognition system.

To analyze the effect of the mismatched centers, the digital patterns of "A," "B," "C," and the patterns "A" shifted by one, two, and three pixels are tested. Fig. 12 shows the measured results. It is easily found that the errors of the shifted patterns are larger when the shifted distance is longer. However, there is still enough difference between the output curves of the shifted patterns to distinguish them from the other two patterns "B" and "C."

In practice, the weight function in (12) and (13) can be adjusted to optimize the output performance. For simplicity,

TABLE I
MEASURED CHARACTERISTICS OF THE FABRICATED R_m AMPLIFIER

Control Voltage (V_{CN}=-V_{CP})	+2.5V ~ -0.9V
Transresistance (r_m)	919 Ohm ~ 1914 Ohm
Input Impedance (r_{in})	44.6 Ohm ~ 88.2 Ohm
Output Impedance (r_o)	2.34 Ohm ~ 44.6 Ohm
-3dB Frequency (f_{-3db})	246.3 MHz ~ 97.4 MHz

TABLE II
SUMMARY OF THE MEASURED CHARACTERISTICS FOR THE PROPOSED ROTATION-INVARIANT RECOGNITION SYSTEM

Process	0.8 DPDM CMOS
Resolution	32x32
Cell Area	110μmx110μm
Fill Factor	0.13
Digital Input Speed	20MHz

the above measured results are obtained by keeping the same weight value on the all five outputs. However, without adjusting the weight values on different outputs, the measured results still have satisfactory performance. In general, the more the input patterns are used, the more necessary it is to optimize the weight functions.

To measure the performance of the fabricated rotation-invariant system for the real-world images, a low-power He-Ne laser and several lenses are used to generate definite input patterns for test. The regular light source was not used in the experiment for characterization because of the serious scattering which makes the image pattern not well defined [20]. However, since the silicon retina is made of semiconductor silicon, it can function well under regular light. In the test setup, the low-power laser beam is incident upon the lens and then focused on the chip through a mask which defines the input pattern.

To measure the rotation invariance of the input images from the real world, the masks of the letter patterns "A," "B," and "C" are fabricated. Through these masks, the laser can project the letter patterns on the chip. The patterns of the letter "A" rotated by $\pi/10$, $\pi/6$, and $\pi/2$ are also tested. Fig. 13 shows the measured results of these input patterns. The curves of the four rotated versions of "A" are similar, whereas those of the individual letters "A," "B," and "C" are quite different.

The typical measured characteristics of the fabricated R_m amplifier are listed in Table I. Table II gives the summary of the measured results. From both simulation and measurement results, the correct functions of the proposed rotation-invariant pattern recognition system realized in CMOS technology have been successfully verified.

VI. CONCLUSION

A new rotation-invariant pattern recognition system which consists of silicon retina cells and simple current summation circuit is proposed and analyzed. In this system, the image sensing and edge extraction is performed by silicon retina cells, whereas the rotation invariance is achieved by the simple circuit realizing the modified discrete correlation function. Both simulation and measurement results have verified the rotation-invariant property of the proposed system. Since the proposed system has a very compact structure and interconnection, and the resultant chip area is small, it is quite feasible to realize the system with the related image processing neural networks in VLSI. Future research will focus on the performance improvement of the system and the integration with other systems for various image processing applications.

ACKNOWLEDGMENT

The authors would like to acknowledge the suggestions and comments of the reviewers which led to the substantial improvements in this paper and the Chip Implementation Center (CIC) of the National Science Council (NSC) of Taiwan, R.O.C. for their support in chip fabrication.

REFERENCES

[1] D. E. Rumelhart and J. L. McClelland, *Parallel Distributed Processing, 1, 2*. Cambridge, MA: MIT Press, 1986.
[2] D. Goldberg, *Genetic Algorithms in Search, Optimization, and Machine Learning*. Reading, MA: Addison-Wesley, 1989.
[3] A. J. Koivo and N. Houshangi, "Real-time vision feedback for serving robotic manipulator with self-tuning controller," *IEEE Trans. Syst. Man, Cybern.*, vol. 21, no. 1, pp. 134–141, Jan./Feb. 1991.
[4] J. S. Shie and G. D. Chang, "A temporally resolved position sensing device for autofocusing," *Rev. Sci. Instruments*, vol. 62, no. 3, pp. 825–827, Mar. 1991.
[5] T. Oya, H. Hashimoto, and F. Harashima, "Active eye sensing system-predictive filtering for visual tracking," in *Proc. IECOM'93 Int. Conf. Industrial Electronics, Control, and Instrumentation*, vol. 3, 1993, pp. 1718–1723.
[6] S. K. Nayar, H. Murase, and S. A. Nene, "Learning, positioning, and tracking visual appearance," in *Proc. 1994 IEEE Int. Conf. Robotics, Automation*, 1994, vol. 4, pp. 3237–3244.
[7] K. Fukushima, S. Miyake, and T. Ito, "Neocognitron: A neural network model for a mechanism of visual pattern recognition," *IEEE Trans. Syst., Man, Cybern.*, vol. SMC-13, no. 5, pp. 826–834, 1983.
[8] G. A. Carpenter and S. Grossberg, "The ART of adaptive pattern recognition by a self-organizing neural networks," *IEEE Comput.*, vol. 21, no. 3, pp. 77–88, 1988.
[9] B. Widrow, R. G. Winter, and R. A. Baxter, "Layered neural nets for pattern recognition," *IEEE Trans. Acoust., Speech, Signal Processing*, vol. 36, no. 7, pp. 1109–1118, 1988.
[10] M. W. Koch, M. W. Roberts, and S. W. Aiken, "A vision architecture for scale, translation, and rotation invariance," in *Proc. Int. Joint Conf. Neural Networks*, 1990, vol. II, pp. 393–396.
[11] M. B. Reid, L. Spirkovska, and E. Ochoa, "Rapid training of high-order neural networks for invariant pattern recognition," in *Proc. Int. Joint Conf. Neural Networks*, 1989, vol. 1, pp. 689–692.
[12] M. K. Hu, "Visual pattern recognition by moment invariants," *IRE Trans. Inform. Theory*, vol. IT-8, pp. 179–187, 1962.
[13] A. Khotanzad and J. Lu, "Classification of invariant image representations using a neural network," *IEEE Trans. Acoust., Speech, Signal Processing*, vol. 38, no. 6, pp. 1028–1238, 1990.
[14] T. Kohonen, *Self-Organization and Associative Memory*. Berlin: Springer-Verlag, 1984.
[15] Y. N. Hsu, H. H. Arsenault, and Y. Yang, "Digital multiple correlation for pattern recognition," *Appl. Opt.*, vol. 21, no. 4, pp. 616–620, Feb. 1982.
[16] Y. N. Hsu and H. H. Arsenault, "Rotation-invariant digital pattern recognition using circular harmonic expansion," *Appl. Opt.*, vol. 21, no. 22, pp. 4012–4015, Nov. 1982.
[17] ——, "Optical pattern recognition using circular harmonic expansion," *Appl. Opt.*, vol. 21, no. 22, pp. 4016–4019, Nov. 1982.
[18] H. H. Arsenault and Y. N. Hsu, "Rotation-invariant discrimination between almost similar objects," *Appl. Opt.*, vol. 22, no. 1, pp. 130–132, Jan. 1983.
[19] S. E. Budge, *A Rotation-Invariant Image Pattern Classifier*, UMI, 1990.
[20] C. Y. Wu and C. F. Chiu, "A new structure for the silicon retina," in *IEDM Tech. Dig.*, pp. 439–442, Dec. 1992.
[21] ——, "A new structure of the 2-D silicon retina," *IEEE J. Solid-State Circuits*, vol. 30, no. 8, pp. 890–897, Aug. 1995.
[22] P. H. Lu, C. Y. Wu, and M. K. Tsai, "VHF bandpass filter design using CMOS transresistance amplifiers," in *Proc. IEEE Int. Symp. Circuits Systems*, May 1993, pp. 990–993.

Chin-Fong Chiu (S'92–M'97) was born in Taipei, Taiwan, R.O.C., in 1966. He received the Ph.D. degree from the Department of Electronics Engineering, National Chiao-Tung University, Hsinchu, Taiwan, in 1996.

He is now with the Chip Implementation Center, Hsinchu, Taiwan, and is engaged in VLSI circuit design. His main research interests have been in neural networks, pattern recognition, and analog integrated circuits and systems.

Chung-Yu Wu (M'77–SM'95) was born in Chiayi, Taiwan, R.O.C., in 1950. He received the M.S. and Ph.D. degrees from the Department of Electronics Engineering, National Chiao-Tung University, Hsinchu, Taiwan, in 1976 and 1980, respectively.

From 1980 to 1984 he was an Associate Professor in the National Chiao-Tung University. During 1984–1986, he was a Visiting Associate Professor in the Department of Electrical Engineering, Portland State University, Oregon. Since 1987, he has been a Professor in the National Chiao-Tung University. From 1991 to 1995, he was rotated to serve as Director of the Division of Engineering and Applied Science in the National Science Council. Currently, he is the Centennial Honorary Chair Professor at the National Chiao-Tung University. He has published more than 70 journal papers and 100 international conference papers on several topics, including digital integrated circuits, analog integrated circuits, computer-aided design, neural networks, ESD protection circuits, special semiconductor devices, and process technologies. He also has 17 patents including 9 U.S. patents. His current research interests focus on low-voltage low-power mixed-mode integrated circuit design, hardware implementation of visual and auditory neural systems, and RF integrated circuit design.

Dr. Wu is a member of Eta Kappa Nu and Phi Tau Phi. He was awarded the Outstanding Research Award by the National Science Council in 1989 and 1995, the Outstanding Engineering Professor by the Chinese Engineer Association, and the one of the Ten Long-Tun Outstanding Professors by the Long-Tun Association in 1996.